Journal of Dynamics, Monitoring and Diagnostics, 2023, 2, 89-101
https://doi.org/10.37965/jdmd.2023.154

ISTP
RESEARCH ARTICLE

Analytical Modeling and Mechanism Analysis of Time-Varying Excitation for Surface Defects in Rolling Element Bearings

Laihao Yang,[1] Yu Sun,[1] Ruobin Sun,[1] Lixia Gao,[2] and Xuefeng Chen[1]
[1]State Key Laboratory for Manufacturing and Systems Engineering, Xi'an Jiaotong University, Xi'an, China
[2]AECC Sichuan Gas Turbine Establishment, Chengdu, China

(Received 09 January 2023; Revised 11 February 2023; Accepted 20 February 2023; Published online 21 February 2023)

Abstract: Surface defects, including dents, spalls, and cracks, for rolling element bearings are the most common faults in rotating machinery. The accurate model for the time-varying excitation is the basis for the vibration mechanism analysis and fault feature extraction. However, in conventional investigations, this issue is not well and fully addressed from the perspective of theoretical analysis and physical derivation. In this study, an improved analytical model for time-varying displacement excitations (TVDEs) caused by surface defects is theoretically formulated. First and foremost, the physical mechanism for the effect of defect sizes on the physical process of rolling element-defect interaction is revealed. According to the physical interaction mechanism between the rolling element and different types of defects, the relationship between time-varying displacement pulse and defect sizes is further analytically derived. With the obtained time-varying displacement pulse, the dynamic model for the deep groove bearings considering the internal excitation caused by the surface defect is established. The nonlinear vibration responses and fault features induced by surface defects are analyzed using the proposed TVDE model. The results suggest that the presence of surface defects may result in the occurrence of the dual-impulse phenomenon, which can serve as indexes for surface-defect fault diagnosis.

Keywords: analytical model; rolling bearings; surface defects; time-varying excitation; vibration mechanism

I. INTRODUCTION

Rolling element bearing is one of the most critical components in rotating machines, such as aeroengines, wind turbine gearboxes, and high-speed spindles. In practical engineering, the presence of defects in rolling element bearings may result in a significant increase in the bearing vibration level. Therefore, detecting and monitoring the occurrence of bearing defects is crucial for the operational safety assurance of rotating machines. Vibration-based condition monitoring and fault detection methods are the most widely exploited methods for bearing defects, which significantly depends on the successful feature extraction of bearing defects.

According to mechanism analysis and practical experience, surface defects may lead to impulse vibration responses when the rolling element passes through the surface defect. The impulse response amplitude depends on the defect shape and depth, which may directly affect the accuracy of the health condition evaluation for rolling element bearings. At present, circles and squares are often employed to characterize the surface shape of surface defects. As for the circle-shaped surface defects, a single sine or cosine function is often utilized to describe the time-varying displacement excitation (TVDE) induced by defects [1], which can be expressed as follows:

$$\delta_{\mathrm{d}} = \begin{cases} H_{\mathrm{d}} \sin\left(\frac{\pi}{\varphi}(\theta_t - \theta_0)\right), & 0 \le |\mathrm{mod}[\theta_t, 2\pi] - \theta_0| \le \frac{\varphi}{2} \\ 0, & \text{otherwise} \end{cases} \tag{1}$$

As for the square-shaped surface defects, a rectangular window function is usually employed to characterize the time-varying excitation induced by defects [2], which can be expressed as:

$$\delta_{\mathrm{d}} = \begin{cases} H_{\mathrm{d}}, & 0 \le |\mathrm{mod}[\theta_t, 2\pi] - \theta_0| \le \frac{\varphi}{2} \\ 0, & \text{otherwise} \end{cases} \tag{2}$$

where H_{d} indicates the defect depth, θ_0 is the initial location of the defect in the circumferential direction, θ_{t} is the rotational angle of the j^{th} rolling element, and φ indicates the circumferential size of the defect.

In recent decades, numerous investigations have been performed based on trigonometric and rectangular models [3–6]. The topics about the fault mechanism of bearings with surface defect [7–9], the influence of defect on bearing vibration feature evolution [10–15], the nonlinear coupling mechanism of rotor-bearing systems with defect [16–21], and the defect size estimation of rolling element bearings [1,12,22,23] have been well and deeply addressed. However, due to the variety and complexity of defect types and shapes, the TVDE model based on the single function is insufficient to accurately characterize the surface topology feature of surface defects, which can be accounted for as follows. First and foremost, the difference in types and shape topologies of defects makes it challenging to obtain an accurate mathematical expression and physical representation of excitations for all types of defects with only a single function [24–27]. Second, even for one type of defect, the difference in defect sizes may also lead to the variance of time-varying displacement and stiffness excitation. For example, the differences in defect length, width, and depth for the defect with rectangular surface topology

Corresponding authors: Laihao Yang (email: yanglaihao@xjtu.edu.cn); Yu Sun (email: yu.sun@xjtu.edu.cn)

will result in different forms of rolling element-defect interactions and thus affect the time-varying excitations [27]. At last, even though the type and defect sizes are determined, the conditions of rolling element-defect interactions may differ due to the defect direction and locations [28].

As indicated in academic research and engineering application, an accurate defect excitation model for rolling element bearings is necessary to accurately predict vibration characteristics induced by defects, which is significant for the accuracy improvement of early bearing fault diagnosis and defect size estimation. Therefore, it is in urgent demand for the accurate mathematical and physical modeling of surface defects according to the defect shapes and sizes and, further, the formulation of the quantitative function between the defect surface topologies (shape and size) and time-varying excitations. Recently, some scholars explored analytical and numerical methods to promote vibration prediction accuracy. As for the analytical modeling of surface defects, there are mainly two techniques to improve. The first is to theoretically deduce the additional displacement excitation, which enables a more accurate characterization of the time-varying excitation induced by surface defects [24,25,27,29,30]. Another is to introduce the impact effect caused by the collision between the leading and trailing edges of surface defects and rolling elements [2,26,27,31,32]. As for the numerical modeling of surface defects, most are developed based on finite element theory [33–36].

Liu et al. [24,25] conducted a series of studies on the analytical modeling of time-varying excitation induced by surface defects of rolling ball bearings using piecewise functions, which depend on the defect shapes and sizes. In their investigations, the time-varying excitation is assumed to be a piecewise function that can be theoretically calculated based on the rolling element-defect interaction relationship. Based on the proposed time-varying excitation model, they further explored the effects of defect edge topologies [37,38] and offset and bias [28] on bearing vibrations and fault feature evolution. The piecewise modeling method is also extended to the defect modeling of roller bearings [29,30,37,39] and the vibration mechanism analysis of rotor-bearing systems with bearing defects [40]. However, one should note that, in Refs. [24,25], the time-varying displacement during the rolling element roll-in and roll-out of defects is set as the complete-period trigonometric function, which constrains the reasonability and accuracy of the proposed model. Luo et al. [41] and Wu et al. [27] further addressed this issue through the theoretical derivation of the additional displacement induced by surface defects rather than using the assumption in Refs. [24,25], based on which they further investigated the dual-impulse phenomenon of vibration responses and quantitative diagnosis for faulty rolling ball bearings. However, only the effect of defect length is considered in their study.

To further involve the impact of rolling element-defect edge collision, some scholars explored the analytical modeling of impact force when the rolling element rolls in and out of the defect. Luo et al. [26] deduced the impact force induced by the interaction between the rolling element and defect zone based on energy conservation theory. It is assumed that the mechanical energy of the rolling element is conservative during its release of deformation from the entry to impact. Combining the additional TVDE model proposed in Ref. [41], they further addressed the dual-impulse behavior and defect size estimation. Cao et al. [42] proposed a novel method to characterize the impact force of rolling element-defect interaction based on the Hertz contact theory. However, due to the two-DOF dynamic model of rolling bearings adopted in their investigations, the above works may fail to capture the three-dimensional motion effects of rolling elements on bearing vibration. Niu et al. [2,31,32,43] developed a complete dynamic model of rolling bearings with surface defects, which is enabled with the capability of characterizing the three-dimensional motion of all components. In their model, the TVDE is modeled as the half-sine function, and the impact force model is developed using Hertz contact theory. Based on the proposed model, they systematically investigated the effects of three-dimensional motion of balls on bearing vibration behavior [2] and the passing frequencies underlying the influences of condition parameters and defect sizes variation [31]. Based on the complete dynamic model of rolling bearings adopted in Refs. [2,31,32,43], Jiang et al. [44] further addressed the vibration modeling and fault feature analysis of rolling bearings considering the three-dimensional defect area. Some investigations are also dedicated to characterizing the rolling element-defect interaction behavior, including the time-varying displacement and impact force excitations with finite element theory [33–36,45]. However, the complexity of nonlinear contact between the rolling element and surface defect may result in challenging issues such as convergence of nonlinear contact problems, enormous consumption of CPU time, and lack of physical interpretability for numerical simulation results. These sufferings restrict the direct application of finite element theory to dynamic modeling of rolling bearings with surface defects.

The investigations mentioned above significantly promote the development and understanding of theoretical modeling and vibration mechanisms of rolling bearings underlying the effects of surface defects. However, there are following issues remain to be addressed. (i) The state-of-the-art studies only provide the time-varying excitation expression for the rectangular defect with different sizes, while the influence of the defect surface topologies on the time-varying excitations remains to be revealed. (ii) The trigonometric function with the entire period is used to construct the piecewise time-varying excitation model, which is inaccurate because the displacement variation does not fully follow the complete-period trigonometric function. (iii) Only two parameters, that is, the ratio of the ball to defect and the ratio of the length to width of defect, to construct the rules of defect modeling, which is insufficient for accurately characterizing rolling element-defect interactions for all types and sizes of the defect. This study focuses on the theoretical modeling of TVDE and vibration mechanism analysis of rolling bearings with surface defects. The main contributions of this study are as follows. (i) First and foremost, theoretically, the main contribution of this work is to deduce the formulation of TVDE induced by surface defect when the rolling element rolls in and out of the defect zone rather than based on the assumption adopted in Refs. [24,25]. As a result, this paper may provide a more reasonable interpretation of the form for TVDE induced by surface defects. (ii) Second, a more comprehensive defect-type classification criterion is proposed by introducing a new parameter related to defect depth, which enables a more accurate and reasonable defect-type characterization. (iii) An improved analytical time-varying displacement

excitation model (ATVDEM) is proposed by combining the defect-type criterion and the TVDE model during the rolling element roll-in and roll-out of the defect. With the proposed ATVDEM, the vibration responses of rolling bearings with different types of surface defects are analyzed, based on which the feature evolution mechanism of defects is revealed.

The remaining parts of this study are organized as follows. In section 2, the contact relationship between the rolling element and surface defect is analyzed, based on which the defect-type criterion is proposed. In section 3, the time-varying excitation mechanism is first investigated, and the ATVDEM is then proposed. In section 4, the validity of ATVDEM is verified, and the vibration mechanism is anlayzed. The conclusion is summarized in section 5.

II. INNER EXCITATION MECHANISM OF BEARING DEFECT

A. MECHANISM ANALYSIS

It is well known that the surface defect on the bearing grooves will generate an impulse excitation when the rolling element passes through the defect. Achieving the accurate estimation of the impulse excitation is of great significance for the vibration modeling and analysis of rolling element bearings with surface defects. Due to the variance of the surface shape for surface defects, the impulse excitation mechanism may differ from each other. In practical engineering, the surface defect characterized by a rectangular-like surface shape (Fig. 1) is the most common one, which will be discussed in this study, while other types of surface defects are beyond this study's scope.

According to the theoretical analysis in Refs. [24,25], it is easy to figure out that the contact points between the rolling element and defect edges may vary over time when the rolling element pass through the defect surface, as shown in Fig. 1. As can be seen in Fig. 1, the impulse excitation form can be classified into five types according to the defect sizes, as well as the contact points variation law. Their inner excitation mechanism is illustrated as follows.

1) TYPE I. The surface defect labeled by Type I (Fig. 1(a)) is employed to describe the surface crack or single-point defect on the groove, which generally occurs in the early stage of bearing faults. In this case, the defect size (length and width) is much less than the size of the rolling element, that is, $d_{ball} \gg \min(L,B)$. When the rolling element passes through the defect, one assumes that there is only one contact point between the rolling element and surface defects.

2) TYPE II. The defect labeled by Type II (Fig. 1(b)) indicates those defects with a larger size than the one of Type I, such as small-size spalling and dent. In this case, we have the following relationships of $L < B$ and

$$H_d > \min\left\{0.5\left(d_{ball}-\sqrt{d_{ball}^2-L^2}\right),0.5\left(d_{ball}-\sqrt{d_{ball}^2-B^2}\right)\right\} \tag{3}$$

As the rolling element rolls over the defect, the number of contact points changes from 1 (the rolling element passes through the defect entry), then to 2 (the rolling element contacts with the leading and trailing edges simultaneously), and finally to 1 (the rolling element exits the defect region). Another phenomenon worthy of notation is that the rolling element does not come into contact with the defect bottom and side edges.

3) TYPE III. The defect labeled by Type III (Fig. 1(c)) is a specified defect with a square surface shape, that is, $L = B$. One should note that this type can be considered a special one of Type II, and thus the condition of Eq. (3) still makes sense. When the rolling element passes through the defect entry, the rolling element only contacts with the defect leading edge, and thus there is only one contact point. As the rolling element reaches the center axis of the defect, the rolling element simultaneously contacts with the defect's leading edge, trailing edge, and two side edges, and thus four contact points exist. As the rolling element rolls over the defect trailing edge, the number of contact points will return to one again.

4) TYPE IV. With the propagation of the above three types of defects, they may develop into the defect labeled Type IV (Fig. 1(d)). In this case, the relationships of $L > B$ and Eq. (3) make sense. In the beginning, the rolling element passes through the entry, where it only contacts with the defect leading edge, resulting in only one contact point. As the rolling element reaches the two side edges, the contact number changes to 3. After that, the rolling element leaves the leading edge, with only contact with two side edges, thus generating two contact points. While the rolling element touches the trailing edge, the rolling element will simultaneously come into contact with two side edges and the trailing edge. Thus, there exist three contact points. Continuously, the rolling element will exit the defect region; within this period, the rolling element will only contact the trailing edge, and thus only one contact point exists between the rolling element and the defect.

5) TYPE V. This type of defect is often employed to describe a severer surface defect, for example, the large-area spalling, which may be caused by the further expansion

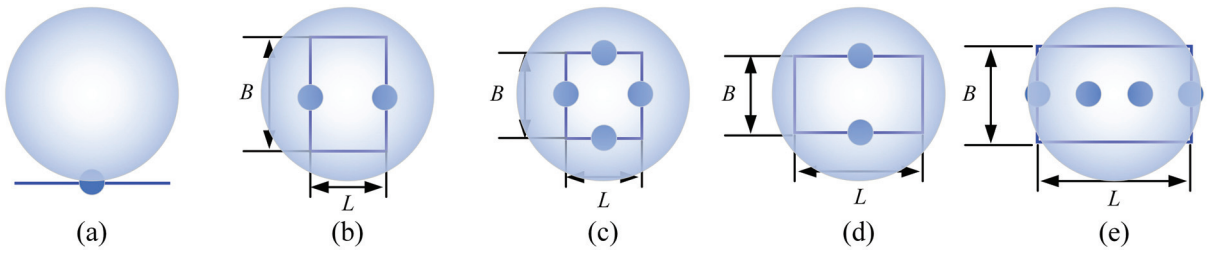

Fig. 1. Contact points between the rolling element and defect, (a) Type I ($d_{ball} \gg \min(L,B)$), (b) Type II ($L < B$), (c) Type III ($L = B$), (d) Type IV ($L > B$), and (e) Type V ($H_d \le H_{sd}$), where d_{ball} denotes the diameter of rolling element.

of the types of defects mentioned above. The defect can be classified as Type V only if the defect size satisfies either of the following two relationships:

$$d_{\text{ball}} \le \min(B,L) \text{ or } H_{\text{d}} \le \min\left\{0.5\left(d_{\text{ball}} - \sqrt{d_{\text{ball}}^2 - L^2}\right), 0.5\left(d_{\text{ball}} - \sqrt{d_{\text{ball}}^2 - B^2}\right)\right\} \tag{4}$$

As shown in Fig. 1(e), there is only one contact point in the beginning during the rolling element passing through the entry. However, when the rolling element touches the bottom of the defect, the contact points will instantly change from 1 to 2. As the rolling element leaves the leading edge, there will be only one contact point again between the rolling element and the defect bottom. As the rolling element reaches the trailing edge, it will generate two pairs of contact between the rolling element and bottom and between the rolling element and trailing edge, respectively. Continuously, the rolling element will leave the bottom and only contact with the trailing edge; thus, only one pair of contact will be generated between the rolling element and the trailing edge.

B. DEFECT-TYPE CRITERIA

In Refs. [24,25], two parameters are employed to mathematically characterize the surface topologies of surface defect for rolling bearings. They are defined as follows:

➢ The ratio of rolling element size to the surface defect size, i.e.,

$$\eta_{\text{bd}} = \frac{d_{\text{ball}}}{\min(B,L)} \tag{5}$$

➢ The ratio of defect length to defect width, i.e.,

$$\eta_{\text{d}} = \frac{L}{B} \tag{6}$$

To characterize the defect types more accurately, in this study, a parameter based on the defect depth is further proposed as follows:

$$\eta_{\text{h}} = \frac{H_{\text{d}}}{\min\left\{0.5\left(d_{\text{ball}} - \sqrt{d_{\text{ball}}^2 - L^2}\right), 0.5\left(d_{\text{ball}} - \sqrt{d_{\text{ball}}^2 - B^2}\right)\right\}} \tag{7}$$

According to the theoretical analysis in the last subsection, one may conclude that (i) the defect should be classified as one of Types II~IV when $\eta_{\text{h}} > 1$ and other additional conditions make sense, and (ii) but when $\eta_{\text{h}} \le 1$, the defect should be classified into Type V.

According to the above-defined parameters, the following criteria can be obtained for the mathematical characterization of the surface defects with rectangular-like surface shape, and it is formulated as:

$$J_{\text{defect type}} = \begin{cases} I & \eta_{\text{bd}} \gg 1, \text{in this study, we set } \eta_{\text{bd}} \ge 200 \\ \text{II} & \eta_{\text{bd}} > 1, \eta_{\text{d}} < 1 \text{ and } \eta_{\text{h}} > 1 \\ \text{III} & \eta_{\text{bd}} > 1, \eta_{\text{d}} = 1 \text{ and } \eta_{\text{h}} > 1 \\ \text{IV} & \eta_{\text{bd}} > 1, \eta_{\text{d}} > 1 \text{ and } \eta_{\text{h}} > 1 \\ V & \eta_{\text{bd}} \le 1 \text{ or } \eta_{\text{h}} \le 1 \end{cases} \tag{8}$$

where $J_{\text{defect type}}$ indicates the label of defect type. Compared with Refs. [24,25], with the introduction of η_{h}, we can better describe and characterize the defect topologies. Significantly, the defect labeled by Type V is characterized by setting $\eta_{\text{bd}} \le 1$ in Refs. [24,25], which is unreasonable and inaccurate because the possibility of the case satisfying the relationship $\eta_{\text{bd}} \le 1$ is rare in practical engineering. Actually, according to Eq. (8), it is easy to be figured out that the defect can be characterized with the label of Type V as long as $\eta_{\text{h}} \le 1$, no matter how much η_{d} is, and $\eta_{\text{bd}} \le 1$ is only the special case for $\eta_{\text{h}} \le 1$.

III. TVDE MODELING

In this section, TVDE will be theoretically formulated based on the defect-type criteria in the last section, thus proposing the improved analytical model for the time-varying displacement excitation model (ATVDEM). With the proposed ATVDEM, the dynamic model of rolling bearings with surface defects will also be developed on the following assumptions. (i) This study focuses on the time-varying displacement induced by surface defects. Thus, the effects of lubrication are neglected. (ii) In order to simplify the modeling process, the 2-DOF dynamic model is employed to develop the vibration model of rolling element bearings with surface defects. Therefore, the three-dimensional motion effects are ignored.

A. IMPROVED ANALYTICAL MODEL FOR TVDE

In conventional investigations, the TVDE is often assumed as a rectangular function [2] or a complete triangle function [24,25], which is not precise in practical engineering. In order to obtain the accurate excitation formulation induced by surface defects, the relative location and motion relationship among groove, rolling element, and defect are detailly analyzed first by taking the defects on the outer groove for instance, as shown in Fig. 2. In Fig. 2, O_{i} is the center of the inner ring. In this study, the center of the inner ring coincides with the outer ring. O_{b}^1 indicates the center location for rolling element when the rolling element starts to pass through the defect entry. O_{b}^2 represents the center point of rolling element after a rotation of θ_j with respect to O_{i} for the rolling cage. R_{i}

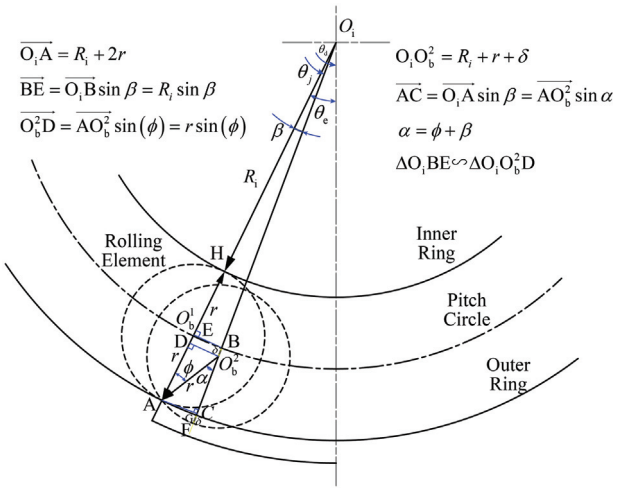

Fig. 2. The geometric relationship among groove, rolling element, and defect when the rolling element passes through the defect.

and r are the radius of inner ring and rolling element, respectively. θ_d indicates the initial location. θ_e represents total angle corresponding to the circumstantial distance of the defect. θ_e can be calculated as follows:

$$\theta_e = \arcsin\left(\frac{L}{2R_i}\right) \tag{9}$$

As shown in Fig. 2, it is easy to figure out the relationship among β, θ_e, θ_d, and θ_j shown as follows:

$$\beta = \theta_e - |\mathrm{mod}(\theta_j, 2\pi) - \theta_d| \tag{10}$$

Considering the geometric relationship as shown in Fig. 2, we can calculate the time-varying displacement induced by the defect as follows:

$$\delta = (R_i + 2r)\cos(\beta) - r\cos(\alpha) - (R_i + r) \tag{11}$$

Since $\Delta O_i AC$ and $\Delta O_b^2 AC$ have the same side AC and AC is perpendicular to the sides CO_i andCO_b^2, thus one can obtain the following relationship:

$$\overrightarrow{AC} = (R_i + 2r)sin(\beta) = rsin(\alpha) \tag{12}$$

Substituting Eq. (12) into Eq. (11) and considering $\alpha \in [0,90^\circ]$, δ can be further expressed as the function of β, ultimately:

$$\begin{aligned}\delta = f(\cos(\beta)) &= (R_i + 2r)\cos(\beta) - (R_i + r) \\ &- \sqrt{r^2 - (R_i + 2r)^2 + (R_i + 2r)^2\cos^2(\beta)}\end{aligned} \tag{13}$$

where $\beta \in [0,\theta_e]$, and thus we have $\cos(\beta) \in [\cos(\theta_e),1]$.

By substituting $\cos(\beta)$ with a variable ζ, we can further simplify Eq. (13) as:

$$\begin{aligned}\delta = f(\zeta) &= (R_i + 2r)\zeta - (R_i + r) \\ &- \sqrt{r^2 - (R_i + 2r)^2 + (R_i + 2r)^2\zeta^2}\end{aligned} \tag{14}$$

where $\zeta = \cos(\beta) \in [\cos(\theta_e),1]$. Furthermore, since the defect size is much smaller than the bearing size, thus θ_e, as well as $\cos(\theta_e)$, is infinitesimal. Therefore, the displacement δ can be expanded near $\zeta = \cos(\beta) = 1$ within the interval of $[\cos(\theta_e),1]$ with the Taylor series. Ignoring the higher-order terms, Eqs. (13)~(14) can be further simplified as:

$$\begin{aligned}\delta &= \frac{(R_i + 2r)(R_i + r)}{r}(1 - \cos(\beta)) \\ &= C_{oe}(1 - \sin(\frac{\pi}{2} - \beta))\end{aligned} \tag{15}$$

where $C_{oe} = \frac{(R_i+2r)(R_i+r)}{r}$. As seen from Eq. (15), it can be figured out that the variation of TVDE follows the sinusoidal function, as shown in Fig. 3.

As shown in Fig. 3, it can be noted that the time-varying displacement functions are symmetrically distributed when the rolling element enters and exits the defect. When the rolling element reaches the leading edge, we have $\mathrm{mod}(\theta_j,2\pi) = \theta_d - \theta_e$, and thus $\beta = 0$. According to Eq. (15), we have $\delta = 0$. For the defect with a smaller length, the rolling element will impact the trailing edge when it reaches the defect center, that is, $\mathrm{mod}(\theta_j,2\pi) = \theta_d$, and thus $\beta = \theta_e$. According to Eq. (15), the TVDE can be estimated as $\delta = C_{oe}(1 - \sin(0.5\pi - \theta_e))$ that is the maximum of the time-varying displacement during the period when the rolling element passes through the defect. After that, as the rolling element exits the defect, the TVDE amplitude will decrease to 0, as shown in Fig. 3(a). This case can be used to characterize the TVDEs induced by the defects labeled with Type II or Type III. For the defect with a larger length, the curve shape of TVDE is similar to the one shown in Fig. 3(a) when the rolling element enters and exits the effect. The maximum excitation amplitude is obtained when $\mathrm{mod}(\theta_j,2\pi) = \theta_d \pm (\theta_e - \theta_{dc})$ rather than $\mathrm{mod}(\theta_j,2\pi) = \theta_d$, which is different from the case shown in Fig. 3(a). As the rolling element leaves the leading edge and does not reach the trailing edge, that is, $\mathrm{mod}(\theta_j,2\pi) \in [\theta_d - (\theta_e - \theta_{dc}),\theta_d + (\theta_e - \theta_{dc})]$, the excitation amplitude will keep constant at $\delta = C_{oe}(1 - \sin(0.5\pi - \theta_{dc}))$, as shown in Fig. 3(b). This case can be used to characterize the TVDE induced by the defects labeled with Type IV or Type V.

In order to further explain the contribution and novelty of this study, the model proposed in Refs. [24,25] is also shown in Fig. 3 (see the red color-marked curve). Due to the absence of detailed analysis and in-depth understanding of

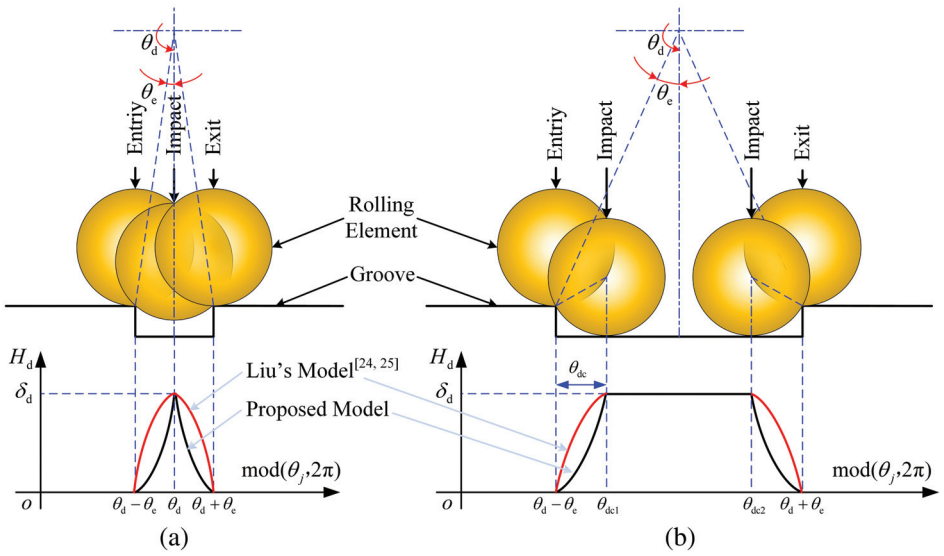

Fig. 3. The proposed time-varying displacement excitation model: (a) semi-sine function, (b) piecewise function.

the contact process between the rolling element and defect, the defect model in Refs. [24,25] only characterize the TVDEs through conventionally empirical formulations. In their model, the TVDE is characterized by the assumed half-period sine function that can be expressed with Eq. (1). The variation of TVDE in Refs. [24,25] is shown with the red color-marked curve in Fig. 3. However, the TVDE of the proposed model in this paper is rigorously formulated through mathematical derivation. As shown with the black color-marked curve in Fig. 3, the proposed TVDE model can be characterized by an inverted sine function that only contains a short period rather than the half-period sine function utilized in Refs. [24,25].

Actually, the formulation of the TVDE can be obtained by analyzing the motion of the rolling element when it rolls over the defect, as shown in Fig. 4. For convenience, the contact deformation of the defect is ignored during the motion analysis. Thus, the displacement variation of the rolling element can be described through the motion of the center of the rolling element, that is, O_b. As seen in Fig. 4, we can note that the process of the rolling element entering the defect can be regarded as a circular motion of the point O_b, where contact point A serves as the center. The contact state change happens until the rolling element entirely enters the defect. Therefore, the motion trajectory of the point O_b can be described with the arc $O_b^1O_b^4$, where contact point A is the center and r is the radius. Ignoring the position alteration of the inner ring, the TVDE is equal to the distance between the rolling element center and the pitch circle in radial direction, that is, $\overrightarrow{M_1O_b^1}$, $\overrightarrow{M_2O_b^2}$, $\overrightarrow{M_3O_b^3}$, and $\overrightarrow{M_4O_b^4}$, as shown in Fig. 4. That is to say, it is unreasonable to quantitatively describe the TVDE with Eqs. (1)-(2). However, in this study, the TVDE is rigorously and mathematically formulated on the basis of geometrical transformation among rolling elements, groove, defect, and Tylor series. The expression of the TVDE when the rolling element enters or exits the defect is then obtained as Eq. (15) that poses more definitely physical meaning and more reasonable calculation result.

B. PIECEWISE FUNCTION MODEL FOR TVDEs

According to the mechanism analysis in section 2, it is worthy of notation that both the differences of defect size and rolling element-defect interaction stage may lead to different kinds of TVDEs during the rolling element passing through defects. Therefore, it is hard to accurately characterize all kinds of TVDEs only using a single piecewise function like Eq. (1)-(2). As indicated in Refs. [24,25], it is necessary to accurately characterize the TVDEs for the defects with different types and sizes using different kinds

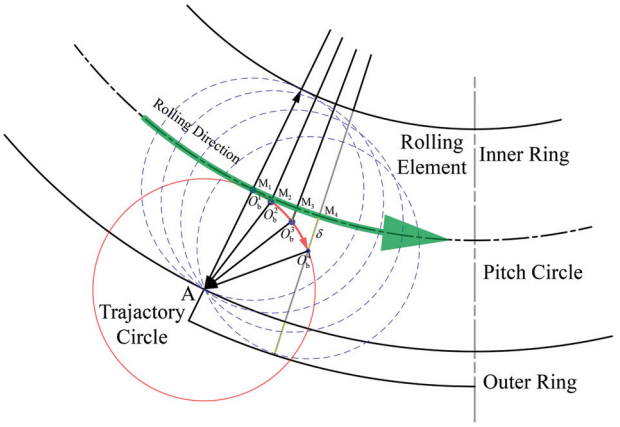

Fig. 4. The schematical diagram of the rolling element-defect contact process.

of piecewise functions. In this study, an improved ATV-DEM characterized by multiple piecewise functions is developed for the rectangular defects with different sizes. Then, the piecewise function models of TVDE for different types of defects are derived and formulated, and they are shown as follows.

1) TYPE I. As for the defect labeled with Type I, all the defect sizes are less than the rolling element sizes, and thus it can be considered as point–point contact between the rolling element and the defect. According to Refs. [24,25], the TVDE induced by rolling element-defect interaction can be expressed as:

$$\delta_d = \begin{cases} C_{oe}^{I}, & \left|\mathrm{mod}\left(\theta_j - 2\pi\right) - \theta_d\right| \le \theta_e \\ 0, & \text{otherwise} \end{cases} \tag{16}$$

where C_{oe}^{I} is the TVDE amplitude, and it can be calculated as follows for the defect labeled with Type I:

$$C_{oe}^{I} = \min\left\{H_d, 0.5\left(d_{ball} - \sqrt{d_{ball}^2 - B^2}\right), \times 0.5\left(d_{ball} - \sqrt{d_{ball}^2 - L^2}\right)\right\} \tag{17}$$

where L, B, and H_d denote the defect length, width, and depth, respectively, and d_{ball} is the diameter of the rolling element.

2) TYPE II. As for the Type II-labeled defects, the TVDE function can be represented as the black-marked curve shown in Fig. 3(a) according to the mechanism analysis in section 2, and it can be expressed as follows:

$$\delta_d = \begin{cases} C_{oe}^{II}[1 - \sin(\frac{\pi}{2} - \theta_e + |\mathrm{mod}(\theta_j - 2\pi) - \theta_d|)], & |\mathrm{mod}(\theta_j - 2\pi) - \theta_d| \le \theta_e \\ 0, & \text{otherwise} \end{cases} \tag{18}$$

where C_{oe}^{II} is the correction factor of TVDE amplitude. In this paper, ignoring higher-order terms for the Tylor series during the formulation of TVDE may introduce estimation error for TVDE, and thus the TVDE amplitude should be modified according to the value of δ_d at $\mathrm{mod}(\theta_j - 2\pi) = \theta_d$. According to the geometrical relationship in Fig. 5, we can obtain $[\delta_d]_{max}^{real} = H_d^{II}$, where $H_d^{II} = 0.5(d_{ball} - \sqrt{d_{ball}^2 - L^2})$. However, according to Eq. (18), it can be obtained that

$$\left[\delta_{\mathrm{d}}\right]_{\max}^{\text{estimation}} = \delta_{\mathrm{d}}\left(\mathrm{mod}\left(\theta_j - 2\pi\right) = \theta_{\mathrm{d}}\right) = C_{\mathrm{oe}}^{\mathrm{II}}\left(1 - \cos\theta_{\mathrm{e}}\right) = H_{\mathrm{d}}^{\mathrm{II}} \tag{19}$$

Further, we can obtain the value of the correction factor as follows:

$$C_{\mathrm{oe}}^{\mathrm{II}} = \frac{1}{1 - \cos\theta_{\mathrm{e}}} H_{\mathrm{d}}^{\mathrm{II}} \tag{20}$$

where $\theta_{\mathrm{e}} = \arcsin\left(L/D_{\mathrm{o}}\right)$ and D_{o} denotes the diameter of the outer ring.

3) TYPE III. Considering $\eta_{\mathrm{d}} = 1$, the defect labeled with Type III is the intermediate state between the defect labeled with Type II and the one labeled with Type IV. The TVDE for these types of defects can be expressed with Eq. (18), and the corresponding correction factor can be calculated with Eq. (20).

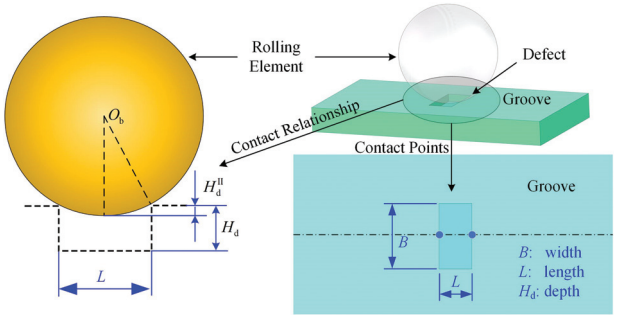

Fig. 5. The schematical diagram of rolling element-defect interaction for the Type II-labeled defect.

4) TYPE IV. As for the Type IV-labeled defects, the TVDE function can be represented as the black-marked curve shown in Fig. 3(b) according to the mechanism analysis in section 2, and it can be expressed as follows:

$$\delta_{\mathrm{d}} = \begin{cases} C_{\mathrm{oe}}^{\mathrm{IV}}[1 - \sin(\frac{\pi}{2} - \theta_{\mathrm{e}} + |\mathrm{mod}(\theta_j - 2\pi) - \theta_{\mathrm{d}}|)], & -\theta_{\mathrm{e}} + \theta_{\mathrm{d}} \le \mathrm{mod}(\theta_j - 2\pi) \le \theta_{\mathrm{dc1}} \\ C_{\mathrm{oe}}^{\mathrm{IV}}(1 - \sin(\frac{\pi}{2} - \theta_{\mathrm{dc}})), & \theta_{\mathrm{dc1}} < \mathrm{mod}(\theta_j - 2\pi) < \theta_{\mathrm{dc2}} \\ C_{\mathrm{oe}}^{\mathrm{IV}}[1 - \sin(\frac{\pi}{2} - \theta_{\mathrm{e}} + |\mathrm{mod}(\theta_j - 2\pi) - \theta_{\mathrm{d}}|)], & \theta_{\mathrm{dc2}} \le \mathrm{mod}(\theta_j - 2\pi) \le \theta_{\mathrm{e}} + \theta_{\mathrm{d}} \\ 0, & \text{otherwise} \end{cases} \tag{21}$$

where $\theta_{\mathrm{dc}} = \arcsin(B/D_{\mathrm{o}})$, $\theta_{\mathrm{dc1}} = \theta_{\mathrm{d}} - \theta_{\mathrm{e}} + \theta_{\mathrm{dc}}$, and $\theta_{\mathrm{dc2}} = \theta_{\mathrm{d}} + \theta_{\mathrm{e}} - \theta_{\mathrm{dc}}$. Similarly, the amplitude coefficient in Eq. (21) can be modified according to the geometrical relationship shown in Fig. 6. It can be obtained that

$$[\delta_{\mathrm{d}}]_{\max} = \delta_{\mathrm{d}}(\mathrm{mod}(\theta_j - 2\pi) \in [\theta_{\mathrm{dc1}}, \theta_{\mathrm{dc2}}]) = C_{\mathrm{oe}}^{\mathrm{IV}}(1 - \cos\theta_{\mathrm{dc}}) = H_{\mathrm{d}}^{\mathrm{IV}} \tag{22}$$

Thus, we have

$$C_{\mathrm{oe}}^{\mathrm{IV}} = \frac{1}{1 - \cos\theta_{\mathrm{dc}}} H_{\mathrm{d}}^{\mathrm{IV}} \tag{23}$$

where $H_{\mathrm{d}}^{\mathrm{IV}} = 0.5\left(d_{\mathrm{ball}} - \sqrt{d_{\mathrm{ball}}^2 - B^2}\right)$.

5) TYPE V. As for the Type V-labeled defects, the TVDE function can be represented as the black-marked curve shown in Fig. 3(b) according to the mechanism analysis in section 2, and it can be expressed as follows:

$$\delta_{\mathrm{d}} = \begin{cases} C_{\mathrm{oe}}^{\mathrm{V}}[1 - \sin(\frac{\pi}{2} - \theta_{\mathrm{e}} + |\mathrm{mod}(\theta_j - 2\pi) - \theta_{\mathrm{d}}|)], & -\theta_{\mathrm{e}} + \theta_{\mathrm{d}} \le \mathrm{mod}(\theta_j - 2\pi) \le \theta_{\mathrm{dc1}} \\ C_{\mathrm{oe}}^{\mathrm{V}}(1 - \sin(\frac{\pi}{2} - \theta_{\mathrm{dc}})), & \theta_{\mathrm{dc1}} \le \mathrm{mod}(\theta_j - 2\pi) \le \theta_{\mathrm{dc2}} \\ C_{\mathrm{oe}}^{\mathrm{V}}[1 - \sin(\frac{\pi}{2} - \theta_{\mathrm{e}} + |\mathrm{mod}(\theta_j - 2\pi) - \theta_{\mathrm{d}}|)], & \theta_{\mathrm{dc2}} \le \mathrm{mod}(\theta_j - 2\pi) \le \theta_{\mathrm{e}} + \theta_{\mathrm{d}} \\ 0, & \text{otherwise} \end{cases} \tag{24}$$

where $\theta_{\mathrm{dc}} = \arccos[(D_{\mathrm{o}} - 2H_{\mathrm{d}})/D_{\mathrm{o}}]$, $\theta_{\mathrm{dc1}} = \theta_{\mathrm{d}} - \theta_{\mathrm{e}} + \theta_{\mathrm{dc}}$, and $\theta_{\mathrm{dc2}} = \theta_{\mathrm{d}} + \theta_{\mathrm{e}} - \theta_{\mathrm{dc}}$. Different from the Type IV-labeled defects, the values of θ_{dc1} and θ_{dc2} are limited by H_{d}. According to the geometrical relationship shown in Fig. 7, we have the following relationship:

$$\left[\delta_{\mathrm{d}}\right]_{\max} = \delta_{\mathrm{d}}\left(\mathrm{mod}\left(\theta_j - 2\pi\right) \in \left[\theta_{\mathrm{dc1}}, \theta_{\mathrm{dc2}}\right]\right) = C_{\mathrm{oe}}^{\mathrm{V}}\left(1 - \cos\theta_{\mathrm{dc}}\right) = H_{\mathrm{d}}^{\mathrm{V}} \tag{25}$$

Then, we have

$$C_{\mathrm{oe}}^{\mathrm{V}} = \frac{1}{1 - \cos\theta_{\mathrm{dc}}} H_{\mathrm{d}}^{\mathrm{V}} \tag{26}$$

where $H_{\mathrm{d}}^{\mathrm{V}} = H_{\mathrm{d}}$.

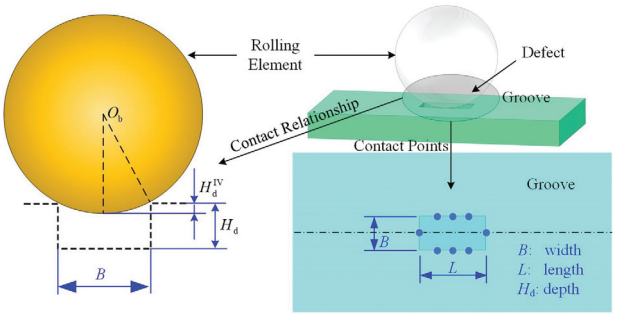

Fig. 6. The schematical diagram of rolling element-defect interaction for the Type IV-labeled defect.

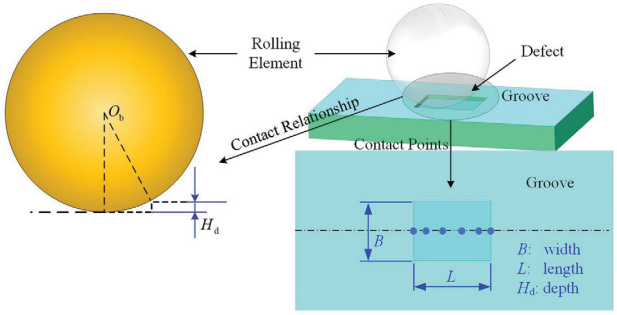

Fig. 7. The schematical diagram of rolling element-defect interaction for the Type IV-labeled defect.

C. DYNAMIC MODELING OF ROLLING ELEMENT BEARINGS WITH DEFECT-INDUCED TVDE

Based on the 2-DOF vibration model for rolling element bearings, the vibration model for the rolling element bearings considering the surface defect can be established by coupling the TVDE model proposed in section 3.2:

$$\begin{cases} m\ddot{x}+c\dot{x}+\sum_{j}^{N_{\text{ball}}}k_{\text{e}}\lambda_j(x\cos\theta_j+y\sin\theta_j-c_{\text{d}}-\delta_{\text{d}})^{n_{\text{e}}}\cos\theta_j=w_x \\ m\ddot{y}+c\dot{y}+\sum_{j}^{N_{\text{ball}}}k_{\text{e}}\lambda_j(x\cos\theta_j+y\sin\theta_j-c_{\text{d}}-\delta_{\text{d}})^{n_{\text{e}}}\sin\theta_j=w_y \end{cases} \tag{27}$$

where m is the equivalent mass of rotor system, c is the damping coefficient, and k_{e} is the total stiffness coefficient for the contact between rolling element and inner/outer grooves. c_{d} is the initial clearance of the rolling element bearing, and δ_{d} denotes the TVDE induced by the surface defect, which can be calculated according to the analysis in subsection 3.2. w_x and w_y denote the directional component of the external load applied on the inner ring of rolling element bearings. λ_j is the Heaviside function that can be expressed as:

$$\lambda_j=\begin{cases}1 & x\cos\theta_j+y\sin\theta_j-c_{\text{d}}-\delta_{\text{d}}\geq 0\\ 0 & \text{otherwise}\end{cases} \tag{28}$$

Combining the proposed TVDE model, the dynamic differential equation shown as Eq. (27) can be solved by the Runge–Kutta method, as shown in Fig. 8.

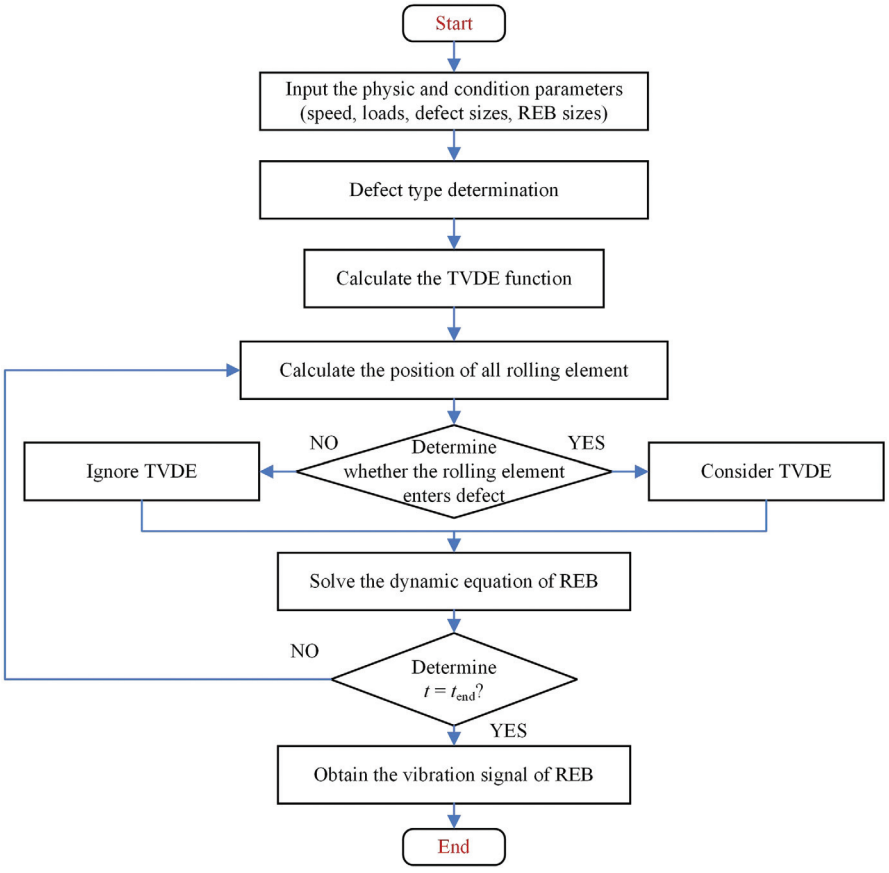

Fig. 8. The schematical diagram for the solution of the dynamic equation of rolling element bearings with the surface defect.

IV. RESULTS AND DISCUSSION

In this section, the proposed ATVDEM is verified by comparing the vibration responses obtained by the proposed ATVDEM and conventional models. Taking the deep groove ball bearing # 6308 as an example, the physical mapping relationship between the defect shape and size and the vibration responses of the rolling element bearing is further investigated. The geometrical and physical parameters adopted in the numerical simulations are listed in Table I. The vibration responses can be obtained with the Runge-Kutta method-based algorithm shown in Fig. 8. In order to obtain a convergent solution, the iteration step is set as 4.8828×10^{-6} s.

A. COMPARISON ANALYSIS AND VERIFICATION

In this study, we consider the surface defect with a length of 0.2 mm, width of 0.08 mm, and depth of 0.004 mm on the outer groove to perform the comparative analysis and verification of different dynamic models for the surface defect. The vibration responses are obtained under the rotating speed of 500 rev/min. Figures 9, 10 present the time-domain waveforms and envelope spectrums of the vibration accelerations, respectively. Figure 11 captures the detail of the behavior when the rolling element rolls in and rolls out of the defect.

The varying compliance (VC) vibration that is similar to the impulse vibration of defect bearings may be observed in the vibration responses of the normal bearing from Fig. 9. This phenomenon is attributed to the VC phenomenon induced by the periodically time-varying loading region, which is also observed in Refs. [46,47]. The corresponding frequency is the so-called VC vibration frequency or the outer ring passing frequency, which can be calculated as follows:

$$f_{\mathrm{VC}} = \frac{1}{2\pi}\omega_{\mathrm{cage}} N_{\mathrm{ball}} = \frac{1}{2\pi}\frac{R_{\mathrm{in}} N_{\mathrm{ball}}}{R_{\mathrm{in}} + R_{\mathrm{out}}}\omega_{\mathrm{shaft}} = 25.6\,\mathrm{Hz} \quad (29)$$

As seen in the spectrums shown in Fig. 10, the corresponding VC vibration frequency is 25.3 Hz, consistent with the theoretical result obtained from Eq. (29). Whereas the errors between the theoretical result and numerical result come from the limitation of low sampling points.

Table I. Rolling element bearing parameters

Item	Value
Equivalent mass m /kg	0.6
Damping coefficient c /N·s·m^{-1}	400
Number of rolling element z	8
Inner ring diameter D_{i} /mm	49.912
Outer ring diameter D_{o}/mm	80.088
Rolling element diameter d /mm	15.081
Pitch diameter d_{m} /mm	65.000
Inner groove curvature radius r_{i} /mm	7.665
Outer groove curvature radius r_{o} /mm	8.010
Radial clearance C_{d} /mm	0.008
Contact angle α /°	0.3
Radial force in horizontal direction w_x /N	0
Radial force in vertical direction w_y /N	20

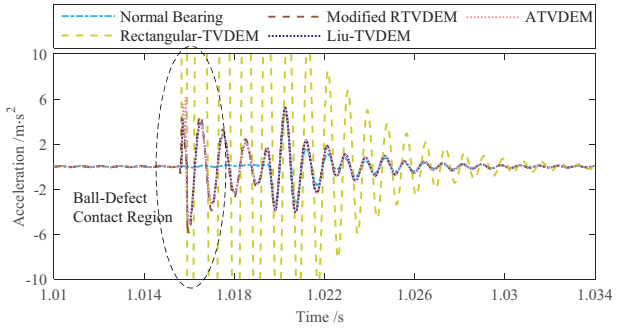

Fig. 9. The waveform of the vibration responses obtained by different surface-defect models.

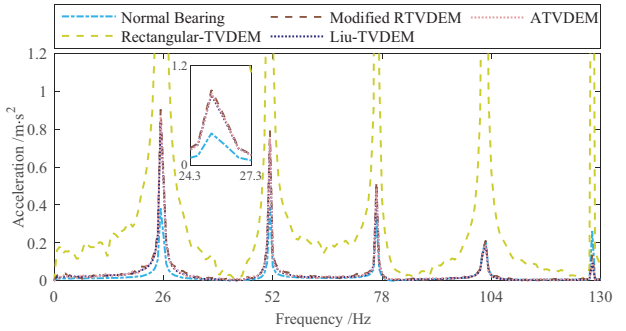

Fig. 10. The spectrums of the bearing vibration accelerations obtained by different surface-defect models.

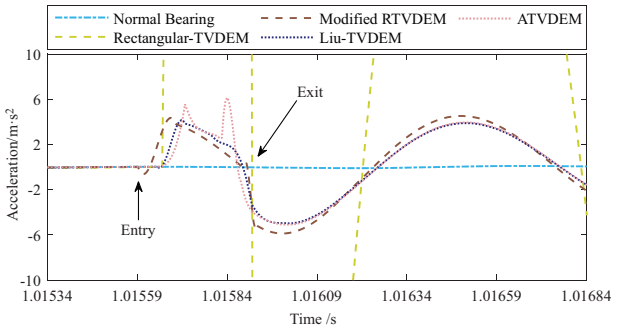

Fig. 11. The zoomed view of the vibration responses in the rolling element-defect contact region.

In order to catch a glimpse of the effect of surface defects on bearing vibration responses further, the vibration responses in the rolling element-defect contact region shown in Fig. 9 is zoomed, as shown in Fig. 11. Comparing the vibration responses of normal bearing and defect bearings, one may note that the normal bearing only causes VC vibration (see the dot-dash line), while the defect bearing brings out VC vibration as well as the impulse vibration induced by the defect. Moreover, another phenomenon can be observed from Fig. 10 that the characteristic frequency for the defect on the outer groove equals the VC vibration frequency of normal bearings, that is, 25.3 Hz. It can be noted that the only difference is that the vibration amplitude is significantly enlarged for the bearings with surface defect, which is induced by the impact effect between the rolling element and defect.

In addition, the vibration responses obtained by different defect models are also compared in Figs. 9, 10. As for the rectangular function-based TVDEM (RTVDEM), the additional TVDE induced by the defect remains constant at its depth in 0.004 mm when the rolling element passes through the defect. However, in practical engineering, according to the mechanism analysis in section 2, the defect simulated in this case belongs to the Type IV defect. The maximum TVDE amplitude is limited by $H_{\mathrm{d}}^{\mathrm{IV}} = 0.5(d - \sqrt{d^2 - B^2}) = 0.1061\mu$m, which is much less than the value of defect depth H_{d}. Therefore, the vibration responses obtained by RTVDEM will be significantly overestimated. In other words, the amplitude is larger than the real one, as shown in the green dot line in Figs. 9, 11. Furthermore, the RTVDEM is modified according to the mechanism analysis in section 2, where the displacement excitation is obtained through

$$\delta_{\text{modified RTVDEM}} = \min\left\{H_{\mathrm{d}}, 0.5\left(d - \sqrt{d^2 - B^2}\right), 0.5\left(d - \sqrt{d^2 - L^2}\right)\right\} \tag{30}$$

As shown in Fig. 11, the overestimation problem is well addressed through the modified RTVDEM, and the model accuracy is improved. For the rectangular function adopted, the impulse response will be excited when the rolling element enters the defect. However, as for other defect models, the sine-like trigonometric function is utilized to characterize the TVDE at the period when the rolling element enters or exits the defect, which leads to more smooth vibration response waveforms.

To analyze and verify the ATVEDM proposed in this study, the vibration responses obtained by ATVDEM and TVDEM in Refs. [24,25] (called Liu-TVDEM) are also compared in Figs. 9, 11. It can be noted that the vibration response obtained by Liu-TVDEM is much more smooth than the one obtained by the proposed ATVDEM. This phenomenon can be accounted for through the expression of TVDEM. According to Refs. [24,25], the complete sine function is used to characterize the TVDE when the rolling element enters and exits the defect, which makes it smoothly pass through the entry to constant displacement excitation and then from the constant displacement excitation to the exit. However, as for the ATVDEM proposed in this study, the TVDE when the rolling element enters or exits is characterized by Eq. (15). It is easy to figure out that there exists an abrupt change when the rolling element passes through the time instant at θ_{dc1} or θ_{dc2}. The abrupt change for TVDE will lead to impulse response, that is, acceleration increment. This phenomenon indicates the dual-impulse feature that is also observed in Refs. [26,27].

To further verify the improvement and effectiveness of the proposed ATVDEM, the vibration responses under the following condition (defect length in 0.2 mm, width in 0.3 mm, and depth in 0.0001 mm) are analyzed and compared. The comparative results are shown in Fig. 12. First, analyzing the defect parameters, one may note that the parameters of the illustrated defect match the Type-V defect. However, according to the theoretical analysis in literatures [24,25], the parameters of the illustrated defect indicate that this defect belongs to Type III. As shown in Fig. 12, it is found that the proposed ATVDEM can well characterize the rolling element-defect contact behavior when the rolling element passes through the surface defect.

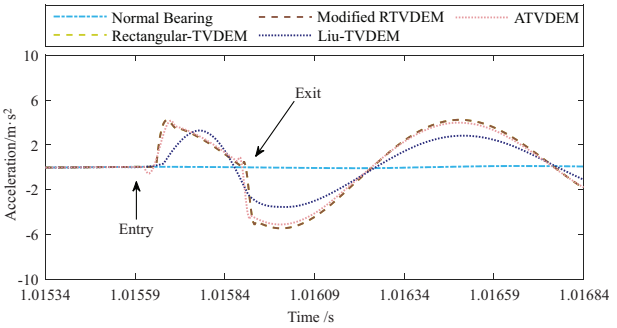

Fig. 12. The comparison of bearing vibration responses obtained under the condition with defect length in 0.2 mm, width in 0.3 mm, and depth in 0.0001 mm.

However, due to the ignorance of defect depth, the inaccurate characterization of TVDE results in the improper estimation of bearing vibration responses. Since Liu-TVDEM [24,25] is developed on the basis of the complete sine function, it is observed that the bearing acceleration also follows the sine function, as shown in Fig. 12. The comparative results indicate that the proposed ATVDEM can well and more comprehensively characterize the TVDE induced by surface defects with different parameters than conventional models do.

B. EFFECTS OF DEFECT SIZE ON VIBRATION RESPONSES

To further investigate the effects of surface defect size on the bearing vibration responses, the proposed ATVDEM is utilized to perform the dynamic simulation, where the defect condition parameters are listed in Table II. According to Eqs. (5)~(8), the defect-type index parameters η_{bd}, η_{d}, and η_{h} are calculated and shown in Table II. And then, the defect types are determined, and they are Type I, II, III, IV, IV, and V, as shown in Table II. The vibration responses are obtained by solving the dynamic equation. The time-domain waveforms and the corresponding spectrums are shown in Figs. 13 and 14, respectively. Figure 15 further presents the zoomed view of the vibration responses at the rolling element-defect contact region. It can be noted from Figs. 13 and 14 that the impulse response component in the vibration acceleration responses increases with the increasing defect length. Moreover, by comparing the frequency spectrums of the acceleration responses obtained under different defect conditions, it can be observed that the amplitude of the fault characteristic frequency component also increases with the increase of defect length. The mechanism for the effect of defect size on the vibration responses will be detailedly analyzed further as follows.

As for the defect condition 1 (Type I), the defect sizes are very small, and thus the amplitudes of the impulse responses are very weak, as shown in Figs. 13 and 14. With the increase of defect length, when $L = 0.08$ mm, that is, defect condition 2, the defect type turns into Type II. Meanwhile, a more obvious impulse response is present in the vibration responses, as shown in Figs. 13 and 15. However, the fault feature remains relatively weak. As shown in Fig. 14, the amplitude of the fault feature component for defect condition 2 and the one for defect condition

Table II. Defect condition parameters

Condition number	*L*/mm	*B*/mm	*H*/mm	η_{bd}	η_d	η_h	Defect type
1	0.04	0.2	0.004	377.025	0.20	6.0321	I
2	0.08	0.2	0.004	188.513	0.40	6.0321	II
3	0.20	0.2	0.004	75.4050	1.00	6.0321	III
4	0.32	0.2	0.004	75.4050	1.60	2.3561	IV
5	0.45	0.2	0.004	75.4050	2.25	1.1913	IV
6	0.45	0.2	0.0006	75.4050	2.25	0.1787	V

1 are at the same level. As the defect length gets more significant to 0.2 mm (defect condition 3), it propagates to the Type III defect. The impulse response amplitude will be apparently increased (see Figs. 13, 15). Comparing the vibration responses obtained under defect conditions 2 and 3, it is easy to be found that, besides the impulse response amplitude, the period during the rolling element passing through the defect is also significantly increased. As the defect length increases continuously, the defect type will turn into Type IV (defect conditions 4 and 5), and the period for rolling element-defect contact is further increased. Moreover, as for these conditions, smooth vibration responses exist between the impulse cased by ther entry and exit of the rolling element. This phenomenon can be attributed to the fact that a constant additional displacement excitation presents when the rolling element leaves the leading edge but not reaches the trailing edge, as shown in Fig. 3.

In order to explore the effect of the Type-V defect on the bearing vibration response, it is simulated by reducing the defect depth from 0.004 mm to 0.0006 mm based on

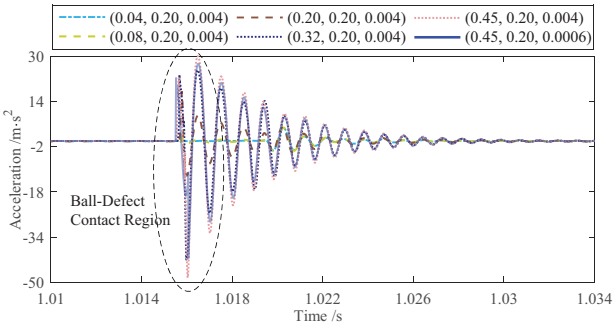

Fig. 13. The waveform of the vibration responses obtained under different defect conditions

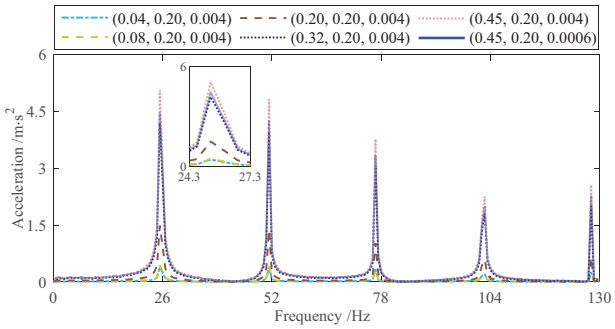

Fig. 14. The spectrums of the bearing vibration accelerations obtained under different defect conditions.

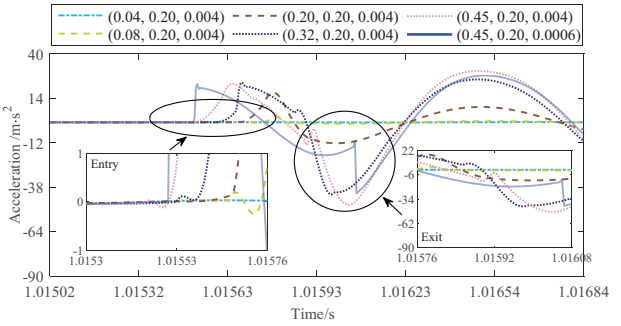

Fig. 15. The zoomed view of the vibration responses at ball-defect contact region.

defect condition 5, and the new defect condition is numbered 6. We have

$$\min\left\{H_d, 0.5\left(d-\sqrt{d^2-L^2}\right), 0.5\left(d-\sqrt{d^2-B^2}\right)\right\} = H_d \tag{31}$$

According to Eq. (8), it is determined that defect condition 6 belongs to the Type-V defect. According to the mechanism analysis in section 2, we have $\theta_{dc}^6 < \theta_{dc}^5$, where the superscript indicates the defection condition number. In other words, the period when the rolling element entirely enters the defect, that is, the period from θ_{dc1} to θ_{dc2} becomes larger for defect condition 6. This phenomenon can be observed in Fig. 15. Moreover, it is worth noting from Fig. 14 that the frequency amplitude obtained under defect condition 6 is smaller than that obtained under defect condition 5. This is caused by the reduction of maximum displacement excitation for defect condition 6 (H_d) compared with defect condition 5 ($0.5(d_{ball} - \sqrt{d_{ball}^2 - L^2})$).

V. RESULTS AND DISCUSSION

This study further addresses the time-varying excitation mechanism of rolling element bearings with surface defects. With the theoretical analysis and numerical investigation, the following conclusions can be summarized:

(I) By addressing the physical mechanism of inner excitation for rolling bearings' surface defect, the TVDE types are fully considered and theoretically revealed. A more general defect-type criteria for rectangular-shaped surface defect is proposed.

(II) With the defect-type criteria, an improved analytical model for TVDE induced by surface defects is developed, where the TVDE is expressed with the multi-piecewise function.

(III) By comparing the vibration responses obtained by different defect models, the validity of the proposed ATVDEM is verified. Some typical fault features, including the passing frequency component and dual impulse, are observed by numerical simulation.

(IV) By exploring the effects of defect size, the propagation law of fault features are revealed. It is found that both the passing frequency amplitude and the rolling element-defect contact period increase with the defect length.

One should note that this study only promotes a small step in improving the TVDE modeling but fails to consider other important factors, such as time-varying stiffness excitation and impact force induced by defects, three-dimensional motion, lubrication, and bearing-rotor coupling, which could be the future direction.

Acknowledgments

This work is sponsored by the National Natural Science Foundation of China (Nos. 52105117 & 52105118).

CONFLICT OF INTEREST STATEMENT

The authors declare no conflicts of interest.

References

[1] M. S. Patil et al., "A theoretical model to predict the effect of localized defect on vibrations associated with ball bearing [J]," Int. J. Mech. Sci., vol. 52, no. 9, pp. 1193–1201, 2010.

[2] L. Niu, H. Cao, and X. Xiong, "Dynamic modeling and vibration response simulations of angular contact ball bearings with ball defects considering the three-dimensional motion of balls[J]," Tribol. Int., vol. 109, pp. 26–39, 2017.

[3] J. Liu and Y. Shao, "Overview of dynamic modelling and analysis of rolling element bearings with localized and distributed faults[J]," Nonlinear Dyn., vol. 93, no. 4, pp. 1765–1798, 2018.

[4] A. Sharma et al., "Nonlinear dynamic investigations on rolling element bearings: a review[J]," Adv. Mech. Eng., vol. 10, no. 3, p. 1687814018764148, 2018.

[5] R. B. Randall and J. Antoni, "Rolling element bearing diagnostics—a tutorial[J]," Mech. Syst. Signal Process., vol. 25, no. 2, pp. 485–520, 2011.

[6] S. G. Kumbhar, P. E. Sudhagar, and R. Desavale, "An overview of dynamic modeling of rolling-element bearings [J]," Noise Vib. Worldwide, vol. 52, nos. 1–2, pp. 3–18, 2021.

[7] Y. Qin et al., "Multiple-degree-of-freedom dynamic model of rolling bearing with a localized surface defect[J]," Mech. Mach. Theory, vol. 154, p. 104047, 2020.

[8] L Zheng, Y Xiang, and C. Sheng, "Nonlinear dynamic modeling and vibration analysis of faulty rolling bearing based on collision impact[J]," J. Comput. Nonlinear Dyn., vol. 16, no. 6, p. 061001, 2021.

[9] S. Lin et al., "A novel dynamic modeling method of defective four-row roller bearings considering the spatial contact correlation between the roller and defect zone[J]," Mech. Mach. Theory, vol. 180, p. 105138, 2023.

[10] C. Mishra, A. K. Samantaray, and G. Chakraborty, "Ball bearing defect models: a study of simulated and experimental fault signatures[J]," J. Sound Vib., vol. 400, pp. 86–112, 2017.

[11] S. Khanam,Vibration Analysis and Feature Extraction of Ball Bearings with Local Defect[D], Indian Institutes of Technology, Delhi, Indian, 2016.

[12] I. Jamadar, "Vibration characteristics diagnosis and estimation of fault sizes in rolling contact bearings: a model-based approach[J]," J. Nondestruct. Eval. Diagn. Progn. Eng. Syst., vol. 5 no. 1, p. 011003, 2022.

[13] H. Zhang et al., "Tracking the natural evolution of bearing spall size using cyclic natural frequency perturbations in vibration signals[J]," Mech. Syst. Signal Process., vol. 151, p. 107376, 2021.

[14] T. Govardhan and A. Choudhury, "Amplitudes of components in vibration spectra of rolling bearings with localized defects under harmonic loads[J]," J. Vib. Control, vol. 27, nos. 13–14, pp. 1537–1547, 2021.

[15] A. R. Bastami and S. Vahid, "A comprehensive evaluation of the effect of defect size in rolling element bearings on the statistical features of the vibration signal[J]," Mech. Syst. Signal Process., vol. 151, p. 107334, 2021.

[16] H. Yu et al., "A time-varying comprehensive dynamic model for the rotor system with multiple bearing faults[J]," J. Sound Vib., vol. 488, p. 115650, 2020.

[17] Y. Yang et al., "Nonlinear vibration signatures for localized fault of rolling element bearing in rotor-bearing-casing system[J]," Int. J. Mech. Sci., vol. 173, p. 105449, 2020.

[18] R. Yang, Z. Zhang, and Y. Chen, "Analysis of vibration signals for a ball bearing-rotor system with raceway local defects and rotor eccentricity[J]," Mech. Mach. Theory, vol. 169, p. 104594, 2022.

[19] P. Gao et al., "Local defect modelling and nonlinear dynamic analysis for the inter-shaft bearing in a dual-rotor system[J]," Appl. Math. Modell., vol. 68, pp. 29–47, 2019.

[20] R. Desavale, J. K. Katiyar, and T. Jagadeesha,Vibrations Characteristics Analysis of Rotor-Bearings System Due to Surface Defects Based in CNC Machines. Recent Advances in Manufacturing, Automation, Design and Energy Technologies: Springer, pp. 705–710, 2022.

[21] T. Gao et al., "Vibration behavior of dual-rotor caused by Maneuver load and intershaft bearing defect[J]," AIAA J., vol. 61, pp. 1–15, 2022.

[22] A. Chen and T. R. Kurfess, "A new model for rolling element bearing defect size estimation[J]," Measurement, vol. 114, pp. 144–149, 2018.

[23] H. Zhang et al., "A benchmark of measurement approaches to track the natural evolution of spall severity in rolling element bearings[J]," Mech. Syst. Signal Process., vol. 166, p. 108466, 2022.

[24] J. Liu, Y. Shao, and T. C. Lim, "Vibration analysis of ball bearings with a localized defect applying piecewise response function[J]," Mech. Mach. Theory, vol. 56, pp. 156–169, 2012.

[25] J. Liu, Y. Shao, and W. Zhu, "A new model for the relationship between vibration characteristics caused by the time-varying contact stiffness of a deep groove ball bearing and defect sizes[J]," J. Tribol., vol. 137, no. 3, p. 031101, 2015.

[26] M. Luo et al., "Dynamic modeling and quantitative diagnosis for dual-impulse behavior of rolling element bearing with a spall on inner race[J]," Mech. Syst. Signal Process., vol. 158, p. 107711, 2021.

[27] R Wu et al., "Dual-impulse behavior analysis and quantitative diagnosis of the raceway fault of rolling bearing[J]," Mech. Syst. Signal Process., vol. 169, p. 108734, 2022.

[28] J Liu et al., "An analytical method for dynamic analysis of a ball bearing with offset and bias local defects in the outer race [J]," J. Sound Vib., vol. 461, p. 114919, 2019.
[29] J. Liu and L. Wang, "Dynamic modelling of combination imperfects of a cylindrical roller bearing[J]," Eng. Failure Anal., vol. 135, p. 106102, 2022.
[30] J. Liu, L. Wang, and Z. Shi, "Dynamic modelling of the defect extension and appearance in a cylindrical roller bearing[J]," Mech. Syst. Signal Process., vol. 173, p. 109040, 2022.
[31] L. Niu et al., "A systematic study of ball passing frequencies based on dynamic modeling of rolling ball bearings with localized surface defects[J]," J. Sound Vib., vol. 357, pp. 207–232, 2015.
[32] L. Niu et al., "Experimental observations and dynamic modeling of vibration characteristics of a cylindrical roller bearing with roller defects[J]," Mech. Syst. Signal Process., vol. 138, p. 106553, 2020.
[33] D. He et al., "Dynamic analysis of rolling bearings with roller spalling defects based on explicit finite element method and experiment[J]," J. Nonlinear Math. Phys., vol. 29, no. 2, pp. 219–243, 2022.
[34] A. Safian et al., "Dynamic simulation of a cylindrical roller bearing with a local defect by combining finite element and lumped parameter models[J]," Meas. Sci. Technol., vol. 32, no. 12, p. 125111, 2021.
[35] S. Singh et al., "Analyses of contact forces and vibration response for a defective rolling element bearing using an explicit dynamics finite element model[J]," J. Sound Vib., vol. 333, no. 21, pp. 5356–5377, 2014.
[36] S. Singh et al., "Analytical validation of an explicit finite element model of a rolling element bearing with a localised line spall[J]," J. Sound Vib., vol. 416, pp. 94–110, 2018.
[37] J. Liu and Y. Shao, "An improved analytical model for a lubricated roller bearing including a localized defect with different edge shapes[J]," J. Vib. Control, vol. 24, no. 17, pp. 3894–3907, 2018.
[38] J. Liu and Y. Shao, "A new dynamic model for vibration analysis of a ball bearing due to a localized surface defect considering edge topographies[J]," Nonlinear Dyn., vol. 79, no. 2, p. 1329–1351, 2015.
[39] Z. Shi, J. Liu, and G. Xiao, "Analysis of cage slip and impact force in a cylindrical roller bearing with race defects[J]," Tribol. Int., vol. 180, p. 108208, 2023.
[40] J. Liu, "A dynamic modelling method of a rotor-roller bearing-housing system with a localized fault including the additional excitation zone[J]," J. Sound Vib., vol. 469, p. 115144, 2020.
[41] M. Luo et al., "An analytical model for estimating spalled zone size of rolling element bearing based on dual-impulse time separation[J]," J. Sound Vib., vol. 453, pp. 87–102, 2019.
[42] B. Cao et al., "New dynamic modelling for a ball bearing system with raceway local defect considering the impact characteristics[C]," 1st International Conference on Mechanical System Dynamics (ICMSD 2022): IET, 2022, pp. 598–606.
[43] L. Niu, "A simulation study on the effects of race surface waviness on cage dynamics in high-speed ball bearings[J]," J. Tribol., vol. 141, no. 5, p. 051101, 2019.
[44] Y. Jiang et al., "A complete dynamics model of defective bearings considering the three-dimensional defect area and the spherical cage pocket[J]," Mech. Syst. Signal Process., vol. 185, p. 109743, 2023.
[45] V. G. Salunkhe, R. G. Desavale, and S. G. Kumbhar, "Vibration analysis of deep groove all bearing using finite element analysis and dimension analysis[J]," J. Tribol., vol. 144, no. 8, p. 081202, 2022.
[46] Z. Zhang, Y. Chen, and Q. Cao, "Bifurcations and hysteresis of varying compliance vibrations in the primary parametric resonance for a ball bearing[J]," J. Sound Vib., vol. 350, pp. 171–184, 2015.
[47] R. Yang et al., "The varying compliance resonance in a ball bearing rotor system affected by different ball numbers and rotor eccentricities[J]," J. Tribol., vol. 140, no. 5, p. 051101, 2018.